

Ferromagnetism, antiferromagnetism, and the curious nematic phase of $S = 1$ quantum spin systems

Daniel Ueltschi*

Department of Mathematics, University of Warwick, Coventry CV4 7AL, United Kingdom

(Received 10 June 2014; revised manuscript received 11 January 2015; published 23 April 2015)

We investigate the phase diagram of $S = 1$ quantum spin systems with $SU(2)$ -invariant interactions, at low temperatures and in three spatial dimensions. Symmetry breaking and the nature of extremal states can be studied using random loop representations. The latter confirm the occurrence of ferro- and antiferromagnetic transitions and the breaking of $SU(3)$ invariance. And they reveal the peculiar nature of the nematic extremal states which minimize $\sum_x (S_x^i)^2$.

DOI: [10.1103/PhysRevE.91.042132](https://doi.org/10.1103/PhysRevE.91.042132)

PACS number(s): 05.30.Rt, 75.10.Jm, 75.30.Gw

I. INTRODUCTION

A fascinating aspect of phase transitions is the notion of symmetry breaking. The set of equilibrium states (infinite-volume Gibbs states) of the system possesses the same symmetries as the Hamiltonian. There is typically a unique Gibbs state at high temperatures which is symmetric. But there may be many different Gibbs states at low temperatures that are not symmetric. An arbitrary state has a unique decomposition in *extremal states*, where extremal states are characterized by their clustering properties (decay of truncated correlation functions) and by the fact that they cannot be decomposed in other states.

The decomposition in extremal states is well described in models such as Ising, where the spin-flip symmetry is broken at low temperatures in dimensions two and higher. Periodic equilibrium states can be written as the convex combination of exactly two periodic extremal states. A similar behavior is expected in models with continuous symmetry, such as the Heisenberg and the XY models. In the case of the classical XY model, there are rigorous results due to Pfister and Fröhlich [1–3].

In this article, we study spin-1 quantum systems with $SU(2)$ -invariant interactions. Let $\Lambda \subset \mathbb{Z}^d$ be a finite lattice, and let $\mathcal{H}_\Lambda = \otimes_{x \in \Lambda} \mathbb{C}^3$ be the Hilbert space of the system. The Hamiltonian is

$$H_\Lambda = - \sum_{(x,y)} (J_1 \vec{S}_x \cdot \vec{S}_y + J_2 (\vec{S}_x \cdot \vec{S}_y)^2), \quad (1)$$

where the sum is over nearest neighbors $x, y \in \Lambda$; the spin operators $S_x^i, x \in \Lambda, i = 1, 2, 3$ satisfy $[S_x^1, S_y^2] = i \delta_{x,y} S_x^3$ (and further cyclic relations) and $(S_x^1)^2 + (S_x^2)^2 + (S_x^3)^2 = 2$. The low-temperature phase diagram for $d \geq 3$ has been investigated by several authors [4–8] and it is expected to split in four regions with ferromagnetic, spin nematic, antiferromagnetic, and staggered nematic phases. They are separated by lines where the model has the larger $SU(3)$ symmetry. See Fig. 1 for an illustration. We investigate it using product states in Sec. II.

There exist mathematically rigorous results that provide a few solid pillars of understanding. The presence of Néel order has been proved for $J_1 < 0, J_2 = 0$, and $d \geq 3$ by Dyson,

Lieb, and Simon [9] using the method of infrared bounds and reflection positivity proposed by Fröhlich, Simon, and Spencer [10]. This result can be straightforwardly extended to small $J_2 > 0$. Quadrupolar order is proved in the spin nematic region for $0 \leq J_1 \leq \frac{1}{2} J_2$ and $d \geq 5$. For J_1 close to $\frac{1}{2} J_2$, the result also holds for $d \geq 3$ [5, 11]. The system has actually Néel order in the direction $J_1 = 0, J_2 > 0$ [11]. Occurrence of quadrupolar order has recently been proved for $J_2 > 0$ and small negative J_1 in $d \geq 6$ [12]; the system should have the stronger Néel order, though.

The goal of this article is to write down the extremal equilibrium states explicitly, and to provide evidence that all (periodic) extremal states have been identified. The method is *exact* in the thermodynamic limit but it is *not rigorous*, as several steps are postulated rather than proved mathematically. We restrict ourselves to $J_2 \geq 0$, where the model possesses probabilistic representations; quantum spin correlations are given by certain random loop correlations. In dimensions three and higher, it has been recently understood that the joint distribution of the lengths of long loops takes a universally simple form, the Poisson-Dirichlet distribution [13], and this allows one to calculate the expectation of certain long-range two-point functions. They can also be calculated using identities from symmetry breaking. These two methods are quite independent and since they must give the same result, they provide a nontrivial test of our understanding.

This strategy has been successfully employed for spin- $\frac{1}{2}$ quantum Heisenberg and XY models [11] and in loop representations of $O(n)$ models [14]. There is in fact little doubt regarding the nature of extremal states and of symmetry breaking in these models. A very interesting aspect of the study of Nahum *et al.* [14] is to give expressions for the moments of long loops and therefore to confirm the presence of the Poisson-Dirichlet distribution.

The phase diagram is worked out in Sec. II using product states. The results of the present article are then explained in Sec. III. The random loop representations are described in Secs. IV and V and the heuristics behind the joint distribution of the lengths of long loops can be found in Sec. VI. It is found that the nature of ferromagnetic and antiferromagnetic phases is as expected. The nature of $SU(3)$ symmetry breaking is less direct, but in retrospect it is also quite expected. The quantum nematic phase, on the other hand, turns out to be surprising; this is explained in Sec. III C.

*daniel@ueltschi.org

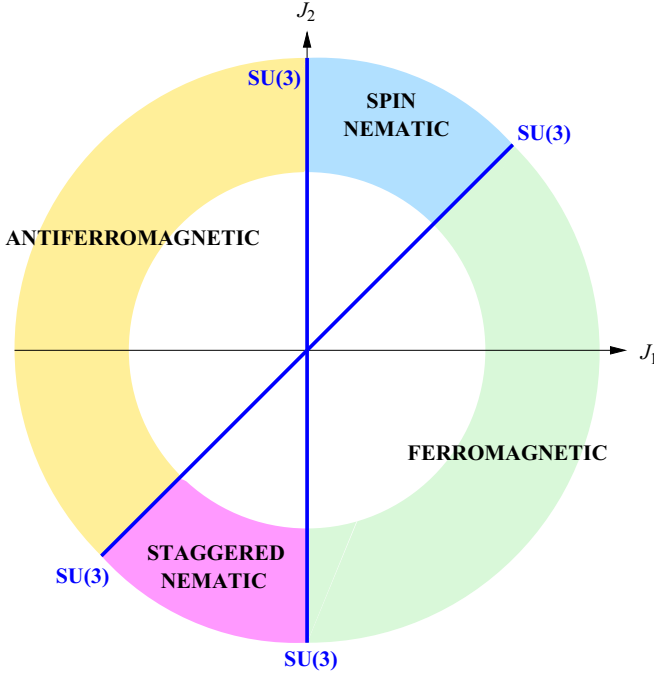


FIG. 1. (Color online) Phase diagram of the spin-1 quantum model with SU(2)-invariant interactions. There are four phases, separated by the lines $J_1 = J_2$ and $J_1 = 0$, where the model has the higher SU(3) symmetry.

II. PHASE DIAGRAM

We study the nearest-neighbor interaction in order to get some understanding of the phase diagram. Let $P_{xy}^{(J)}$, $J = 0, 1, 2$, denote the projector onto the eigensubspace of $(\vec{S}_x + \vec{S}_y)^2$ with eigenvalue $J(J+1)$ (recall that $\text{rank } P_{xy}^{(J)} = 2J+1$). It can be checked that

$$\begin{aligned} J_1 \vec{S}_x \cdot \vec{S}_y + J_2 (\vec{S}_x + \vec{S}_y)^2 \\ = (3J_2 - J_1) P_{xy}^{(0)} + 2J_1 P_{xy}^{(2)} - J_1 + J_2. \end{aligned} \quad (2)$$

But many eigenstates are strongly entangled, so they have little relevance for lattices with more than two sites. A better approach is to consider product states. For this purpose, we write the interaction as a linear combination of $P_{xy}^{(0)}$ and of the transposition operator T_{xy} . The transposition operator is defined by

$$T_{xy}|a, b\rangle = |b, a\rangle, \quad (3)$$

where $a, b = -1, 0, 1$. As for the projector $P_{xy}^{(0)}$, its matrix elements are the Clebsch-Gordon coefficients

$$\langle a, b | P_{xy}^{(0)} | c, d \rangle = \frac{1}{3} (-1)^{a-c} \delta_{a,-b} \delta_{c,-d}, \quad (4)$$

where $a, b, c, d = -1, 0, 1$. These operators can be expressed in terms of spin operators, namely,

$$\begin{aligned} T_{xy} &= \vec{S}_x \cdot \vec{S}_y + (\vec{S}_x + \vec{S}_y)^2 - 1, \\ P_{xy}^{(0)} &= \frac{1}{3} (\vec{S}_x + \vec{S}_y)^2 - \frac{1}{3}. \end{aligned} \quad (5)$$

The interaction then takes the form

$$J_1 \vec{S}_x \cdot \vec{S}_y + J_2 (\vec{S}_x + \vec{S}_y)^2 = J_1 T_{xy} + 3(J_2 - J_1) P_{xy}^{(0)} + J_2. \quad (6)$$

Let $|\varphi, \psi\rangle = |\varphi\rangle \otimes |\psi\rangle$ be a product state, with $\varphi, \psi \in \mathbb{C}^3$. We have

$$\langle \varphi, \psi | T_{xy} | \varphi, \psi \rangle = |\langle \varphi | \psi \rangle|^2. \quad (7)$$

Next, let $\tilde{\psi}$ denote the vector in \mathbb{C}^3 with coefficients

$$\tilde{\psi}_a = (-1)^a \bar{\psi}_{-a}, \quad (8)$$

where $a = -1, 0, 1$. Then

$$\langle \varphi, \psi | P_{xy}^{(0)} | \varphi, \psi \rangle = \frac{1}{3} |\langle \varphi | \tilde{\psi} \rangle|^2. \quad (9)$$

Equations (7) and (9) allow one to find the product states that minimize the interaction $-J_1 \vec{S}_x \cdot \vec{S}_y - J_2 (\vec{S}_x + \vec{S}_y)^2$. There are four cases.

Case $J_1 > 0$, $J_2 - J_1 < 0$. We have $\langle \varphi | \psi \rangle = 1$ and $\langle \varphi | \tilde{\psi} \rangle = 0$. Then $\varphi = \psi$, and the coefficients of φ satisfy

$$\varphi_0^2 - 2\varphi_1 \varphi_{-1} = 0. \quad (10)$$

We get in particular the ferromagnetic states such as $|1\rangle$ and $|-1\rangle$.

Case $J_1 > 0$, $J_2 - J_1 > 0$. We have $\langle \varphi | \psi \rangle = 1$ and $\langle \varphi | \tilde{\psi} \rangle = ei\theta$ with $\theta \in [0, 2\pi]$. Then $\varphi = \psi = ei\theta \tilde{\psi}$. Explicitly, the vectors must satisfy the conditions

$$\varphi_{\pm 1} = -ei\theta \bar{\varphi}_{\mp 1}, \quad \varphi_0 = ei\theta \bar{\varphi}_0. \quad (11)$$

This gives the ‘‘classical’’ nematic state $|1\rangle + |-1\rangle$, but also $|0\rangle$ and such linear combination as $|1\rangle + i|0\rangle + |-1\rangle$.

Case $J_1 < 0$, $J_2 - J_1 > 0$. This is identical to the first case (the ferromagnetic one) if we exchange ψ with $\tilde{\psi}$. We get the same states for φ but the resulting tensor state is $\varphi \otimes \tilde{\varphi}$. This gives in particular the Néel state $|1\rangle \otimes |-1\rangle$.

Case $J_1 < 0$, $J_2 - J_1 < 0$. We have $\langle \varphi | \psi \rangle = \langle \varphi | \tilde{\psi} \rangle = 0$. There are many solutions; we can choose a nematic state that satisfies $\varphi = ei\theta \tilde{\varphi}$, and any state ψ that is orthogonal to φ .

This analysis suggests the phase diagram depicted in Fig. 1.

III. NATURE OF EXTREMAL STATES

Let $\langle \cdot \rangle_{H_\Lambda}$ denote the finite-volume Gibbs state with Hamiltonian H_Λ , where the expectation of the observable A is

$$\langle A \rangle_{H_\Lambda} = \frac{1}{Z_\Lambda} \text{Tr } A e^{-\beta H_\Lambda}, \quad (12)$$

with $Z_\Lambda = \text{Tr } e^{-\beta H_\Lambda}$ the partition function. We let $\langle \cdot \rangle$ denote its infinite-volume limit. Our goal is to identify the extremal states $\langle \cdot \rangle_{\vec{a}}$ such that

$$\langle \cdot \rangle = \int \langle \cdot \rangle_{\vec{a}} d\nu(\vec{a}), \quad (13)$$

where $d\nu$ is a probability measure on the set of possible values for \vec{a} . We describe separately the ferromagnetic, broken SU(3), spin nematic, broken staggered SU(3), and antiferromagnetic phases. In each case we propose a decomposition, use it to calculate the two-point functions, and compare with results obtained with random loop representations. We conclude the section with a discussion of the staggered nematic phase; we make a conjecture but do not provide conclusive evidence.

A. Ferromagnetic phase

This is the simplest situation, valid when parameters satisfy $J_1 > 0$ and $J_2 < J_1$ (see Fig. 1). To each unit vector $\vec{a} \in \mathbb{R}^3$, there corresponds the ferromagnetic extremal state

$$\langle \cdot \rangle_{\vec{a}}^{\text{ferro}} = \lim_{h \rightarrow 0^+} \lim_{\Lambda \rightarrow \mathbb{Z}^d} \langle \cdot \rangle_{H_\Lambda - h \sum_x \vec{a} \cdot \vec{S}_x}. \quad (14)$$

Let \mathbb{S}^2 denote the unit sphere in \mathbb{R}^3 and let $d\nu$ be the uniform probability measure. The infinite-volume state $\langle \cdot \rangle$ should satisfy the identity

$$\langle \cdot \rangle = \int_{\mathbb{S}^2} \langle \cdot \rangle_{\vec{a}}^{\text{ferro}} d\nu(\vec{a}). \quad (15)$$

We can apply this decomposition to the special case of the two-point function $\langle S_x^3 S_y^3 \rangle$ with x, y far apart. We have

$$\begin{aligned} \langle S_x^3 S_y^3 \rangle &= \frac{1}{3} \langle \vec{S}_x \cdot \vec{S}_y \rangle \stackrel{(a)}{=} \frac{1}{3} \int_{\mathbb{S}^2} \langle \vec{S}_x \cdot \vec{S}_y \rangle_{\vec{a}}^{\text{ferro}} d\nu(\vec{a}) \\ &\stackrel{(b)}{=} \frac{1}{3} \langle \vec{S}_x \cdot \vec{S}_y \rangle_{\vec{e}_3}^{\text{ferro}} \stackrel{(c)}{=} \frac{1}{3} \sum_{i=1}^3 \langle S_x^i \rangle_{\vec{e}_3}^{\text{ferro}} \langle S_y^i \rangle_{\vec{e}_3}^{\text{ferro}} \\ &\stackrel{(d)}{=} \frac{1}{3} \langle (\lambda_x^3)_{\vec{e}_3}^{\text{ferro}} \rangle^2. \end{aligned} \quad (16)$$

We have used the following: (a) the conjecture Eq. (15); (b) $\vec{S}_x \cdot \vec{S}_y$ is SU(2)-invariant; (c) extremal states are clustering, hence factorization when $\|x - y\| \gg 1$; (d) translation invariance and $\langle S_x^i \rangle_{\vec{e}_3}^{\text{ferro}} = 0$ for $i = 1, 2$; the latter follows from the rotation invariance around \vec{e}_3 of the extremal state.

We provide independent evidence for the identity (16), and hence (15), using the random loop representation and the conjecture about the joint distribution of the lengths of long loops; see Sec. VIC.

B. Breaking SU(3) invariance

When $J_1 = J_2$ the Hamiltonian has the larger SU(3) symmetry. Indeed, the interaction is given by the transposition operator T_{xy} defined in (3). Given any unitary U in \mathbb{C}^3 , the tensor product $U_\Lambda = \otimes_x U$ commutes with all T_{xy} 's.

The group SU(3) has eight dimensions and it is generated, e.g., by the Gell-Mann matrices $\lambda^1, \dots, \lambda^8$. All matrices have empty diagonal except λ^3 and λ^8 :

$$\lambda^3 = \begin{pmatrix} 1 & 0 & 0 \\ 0 & -1 & 0 \\ 0 & 0 & 0 \end{pmatrix}, \quad \lambda^8 = \frac{1}{\sqrt{3}} \begin{pmatrix} 1 & 0 & 0 \\ 0 & 1 & 0 \\ 0 & 0 & -2 \end{pmatrix}. \quad (17)$$

Another property that is relevant for our purpose is the identity

$$\sum_{i=1}^8 \lambda_x^i \lambda_y^i = 2T_{xy} - \frac{2}{3}, \quad (18)$$

which shows that $\sum_i \lambda_x^i \lambda_y^i$ is SU(3)-invariant. The extremal states are given by

$$\langle \cdot \rangle_{\vec{a}} = \lim_{h \rightarrow 0^+} \lim_{\Lambda \rightarrow \mathbb{Z}^d} \langle \cdot \rangle_{H_\Lambda - h \sum_x \vec{a} \cdot \vec{S}_x}. \quad (19)$$

Here, \vec{a} is a vector in \mathbb{S}^7 , the unit sphere in \mathbb{R}^8 . Let $d\nu$ be the uniform probability measure on \mathbb{S}^7 . The decomposition of the

SU(3)-invariant Gibbs state is

$$\langle \cdot \rangle = \int_{\mathbb{S}^7} \langle \cdot \rangle_{\vec{a}} d\nu(\vec{a}). \quad (20)$$

The two-point function can be calculated as in the ferromagnetic case, Eq. (16):

$$\begin{aligned} \langle S_x^3 S_y^3 \rangle &= \frac{1}{8} \left\langle \sum_{i=1}^8 \lambda_x^i \lambda_y^i \right\rangle = \frac{1}{8} \int_{\mathbb{S}^7} \left\langle \sum_{i=1}^8 \lambda_x^i \lambda_y^i \right\rangle_{\vec{a}} d\nu(\vec{a}) \\ &= \frac{1}{8} \left\langle \sum_{i=1}^8 \lambda_x^i \lambda_y^i \right\rangle_{\vec{e}_3} = \frac{1}{8} \sum_{i=1}^8 \langle (\lambda_x^i)_{\vec{e}_3} \rangle^2 \\ &= \frac{1}{8} \langle (\lambda_x^3)_{\vec{e}_3} \rangle^2 + \frac{1}{8} \langle (\lambda_x^8)_{\vec{e}_3} \rangle^2. \end{aligned} \quad (21)$$

We used the clustering property of extremal states when $\|x - y\| \rightarrow \infty$. We have $\langle \lambda_x^i \rangle_{\vec{e}_3} = 0$ if $i \neq 3, 8$, and $\langle \lambda_x^8 \rangle_{\vec{e}_3} = \frac{1}{\sqrt{3}} \langle \lambda_x^3 \rangle_{\vec{e}_3}$. We obtain

$$\langle S_x^3 S_y^3 \rangle = \frac{1}{6} \langle (\lambda_x^3)_{\vec{e}_3} \rangle^2. \quad (22)$$

We check this identity using the random loop representation in Sec. VIC.

The matrix λ^8 is peculiar, as it is not unitarily equivalent to the other seven matrices. It is worth checking that the corresponding extremal state gives the same result. The second line of Eq. (21) becomes

$$\begin{aligned} \dots &= \frac{1}{8} \left\langle \sum_{i=1}^8 \lambda_x^i \lambda_y^i \right\rangle_{\vec{e}_8} = \frac{1}{8} \sum_{i=1}^8 \langle (\lambda_x^i)_{\vec{e}_8} \rangle^2 \\ &= \frac{1}{8} \langle (\lambda_x^1)_{\vec{e}_8} \rangle^2 + \frac{1}{8} \langle (\lambda_x^8)_{\vec{e}_8} \rangle^2. \end{aligned} \quad (23)$$

It turns out that $\langle \lambda_x^8 \rangle_{\vec{e}_8} = \frac{1}{\sqrt{3}} \langle \lambda_x^1 \rangle_{\vec{e}_8} = \frac{1}{\sqrt{3}} \langle \lambda_x^3 \rangle_{\vec{e}_3}$. This can indeed be seen using the random loop representation. We recover the identity (22).

C. Curious spin nematic phase

In the classical model with $J_1 = 0, J_2 > 0$, there is a spin nematic phase where the classical spins are aligned or antialigned [15,16]. This suggests that extremal states can be defined using an external field of the form $-\sum_x (\vec{a} \cdot \vec{S}_x)^2$. The quantum system is very different for two main reasons. First, the direction $J_1 = 0, J_2 > 0$ is not nematic but it has Néel order [11]; its broken staggered SU(3) invariance is explained in the next subsection. The second reason is that, for $J_2 > J_1 > 0$, extremal states are obtained using the external field $+\sum_x (\vec{a} \cdot \vec{S}_x)^2$ with a “+” sign. Rather than projecting onto the eigenstates of S_x^i with eigenvalues ± 1 , we project onto the eigensubspace with value zero. This is rather surprising and this signals a purely quantum phenomenon.

Let \mathbb{S}_+^2 denote the unit hemisphere in \mathbb{R}^3 with nonnegative third coordinates. Given $\vec{a} \in \mathbb{S}_+^2$, the corresponding extremal state is

$$\langle \cdot \rangle_{\vec{a}}^{\text{nem}} = \lim_{h \rightarrow 0^+} \lim_{\Lambda \rightarrow \mathbb{Z}^d} \langle \cdot \rangle_{H_\Lambda + h \sum_x (\vec{a} \cdot \vec{S}_x)^2}. \quad (24)$$

With $d\nu$ the uniform probability measure on \mathbb{S}_+^2 , the nematic decomposition reads

$$\langle \cdot \rangle = \int_{\mathbb{S}_+^2} \langle \cdot \rangle_{\vec{a}}^{\text{nem}} d\nu(\vec{a}). \quad (25)$$

The spin-spin correlation function is not a suitable order parameter for the nematic phase. Indeed, it certainly has exponential decay, as suggested by its random loop representation; see Eq. (49) below. So we rather pick the observable for quadrupolar order:

$$A_x = (S_x^3)^2 - \frac{2}{3}. \quad (26)$$

Notice that $\langle A_x \rangle = 0$. The calculation of the quadrupolar two-point function can be done in the nematic phase as follows:

$$\begin{aligned} \langle A_x A_y \rangle &= \int_{\mathbb{S}_+^2} \langle A_x A_y \rangle_{\vec{a}}^{\text{nem}} d\nu(\vec{a}) \\ &= \int_{\mathbb{S}_+^2} \left(\left\langle (S_x^3)^2 - \frac{2}{3} \right\rangle_{\vec{a}}^{\text{nem}} \right)^2 d\nu(\vec{a}) \\ &= \int_{\mathbb{S}_+^2} \left(\left\langle (\vec{a} \cdot \vec{S}_x)^2 - \frac{2}{3} \right\rangle_{\vec{e}_3}^{\text{nem}} \right)^2 d\nu(\vec{a}). \end{aligned} \quad (27)$$

The second identity is due to clustering when $\|x - y\| \gg 1$ and the last identity follows by rotating the observable rather than the state. Next, we have

$$\begin{aligned} \left\langle (\vec{a} \cdot \vec{S}_x)^2 - \frac{2}{3} \right\rangle_{\vec{e}_3}^{\text{nem}} &= \sum_{i,j=1}^3 a_i a_j \langle S_x^i S_x^j \rangle_{\vec{e}_3}^{\text{nem}} - \frac{2}{3} \\ &= \sum_{i=1}^3 a_i^2 \left\langle (S_x^i)^2 - \frac{2}{3} \right\rangle_{\vec{e}_3}^{\text{nem}}. \end{aligned} \quad (28)$$

We now use the following identities:

$$\left\langle (S_x^3)^2 - \frac{2}{3} \right\rangle_{\vec{e}_3}^{\text{nem}} = -2 \left\langle (S_x^1)^2 - \frac{2}{3} \right\rangle_{\vec{e}_3}^{\text{nem}} = -2 \left\langle (S_x^2)^2 - \frac{2}{3} \right\rangle_{\vec{e}_3}^{\text{nem}}. \quad (29)$$

They follow from symmetry and from the identity $(S_x^1)^2 + (S_x^2)^2 + (S_x^3)^2 = 2$. We obtain

$$\begin{aligned} \langle A_x A_y \rangle &= \left(\left\langle (S_x^1)^2 - \frac{2}{3} \right\rangle_{\vec{e}_3}^{\text{nem}} \right)^2 \int_{\mathbb{S}_+^2} (a_1^2 + a_2^2 - 2a_3^2)^2 d\nu(\vec{a}) \\ &= \frac{4}{5} \left(\left\langle (S_x^1)^2 - \frac{2}{3} \right\rangle_{\vec{e}_3}^{\text{nem}} \right)^2. \end{aligned} \quad (30)$$

This identity is verified in Sec. VIC using the loop representation.

It is natural to wonder about the states $\langle \cdot \rangle_{\vec{a}}^*$ obtained with external field $-\sum_x (\vec{a} \cdot \vec{S}_x)^2$. If these were the extremal states, one should expect the decomposition $\langle \cdot \rangle = \int_{\mathbb{S}_+^2} \langle \cdot \rangle_{\vec{a}}^* d\nu(\vec{a})$. However, the calculations of $\langle A_x A_y \rangle$ give a result that is incompatible with the random loop calculations, so this has to be discarded. If $\langle \cdot \rangle_{\vec{a}}^*$ are not extremal states, then they should be linear combinations of the nematic states. And indeed, it appears that

$$\langle \cdot \rangle_{\vec{a}}^* = \frac{1}{2\pi} \int_{\vec{b} \perp \vec{a}} \langle \cdot \rangle_{\vec{b}}^{\text{nem}} d\vec{b}. \quad (31)$$

In the case of one-site observables this can be checked using the following identity that holds for all matrices A in \mathbb{C}^3 :

$$\frac{1}{2\pi} \int_{\vec{b} \perp \vec{e}_3} \langle 0 | U_{\vec{b}} A U_{\vec{b}}^* | 0 \rangle d\vec{b} = \frac{1}{2} \text{Tr}(S^3)^2 A. \quad (32)$$

Here, we set $U_{\vec{b}} = e^{i\frac{\pi}{2}(\vec{b} \times \vec{e}_3) \cdot \vec{S}}$. The identity (31) can certainly be verified for more general many-site observables.

D. Breaking staggered SU(3) invariance

In the case $J_1 = 0$, $J_2 > 0$, the interaction is equivalent to the projector onto the spin singlet $P_{xy}^{(0)}$ defined in (4). Given any unitary matrix U in \mathbb{C}^3 , let \tilde{U} denote the matrix with elements

$$\tilde{U}_{a,b} = (-1)^{a-b} \overline{U_{-a,-b}}. \quad (33)$$

Here, $\overline{U_{-a,-b}}$ is the complex conjugate of $U_{-a,-b}$; notice that $\tilde{\tilde{U}} = U$. One can check that

$$P_{xy}^{(0)} U \otimes \tilde{U} = U \otimes \tilde{U} P_{xy}^{(0)} = P_{xy}^{(0)}. \quad (34)$$

As a consequence, the Hamiltonian H_Λ has SU(3) invariance whenever the lattice Λ is bipartite. More precisely, if Λ_A, Λ_B are the two sublattices, the unitary operator on $\otimes_{x \in \Lambda} \mathbb{C}^3$ is

$$U_\Lambda = \otimes_{x \in \Lambda_A} U \otimes_{x \in \Lambda_B} \tilde{U}. \quad (35)$$

On nonbipartite lattices, the Hamiltonian has only SU(2) invariance and the low-temperature phase is the spin nematic phase discussed in the previous subsection.

In the rest of this subsection we restrict ourselves to the bipartite lattice \mathbb{Z}^d , $d \geq 3$. The extremal states can be defined using staggered fields. Given a unit vector \vec{a} in \mathbb{R}^8 , let

$$Q_\Lambda^{\vec{a}} = \sum_{x \in \Lambda_A} \vec{a} \cdot \vec{\lambda}_x + \sum_{x \in \Lambda_B} \vec{a} \cdot \tilde{\vec{\lambda}}_x. \quad (36)$$

As in Sec. IIIB, $\vec{\lambda}_x = (\lambda_x^1, \dots, \lambda_x^8)$ is the vector of Gell-Mann matrices acting on the site x . We also defined $\tilde{\vec{\lambda}}_x = (\tilde{\lambda}_x^1, \dots, \tilde{\lambda}_x^8)$. Then we set

$$\langle \cdot \rangle_{\vec{a}} = \lim_{h \rightarrow 0^+} \lim_{\Lambda \rightarrow \mathbb{Z}^d} \langle \cdot \rangle_{H_\Lambda - h Q_\Lambda^{\vec{a}}}. \quad (37)$$

The decomposition of the symmetric Gibbs state reads

$$\langle \cdot \rangle = \int_{\mathbb{S}^7} \langle \cdot \rangle_{\vec{a}} d\nu(\vec{a}). \quad (38)$$

The justification of this formula mirrors that of Eq. (20) in the nonstaggered SU(3) situation. Without entering details, let us note that

$$\begin{aligned} 3P_{xy}^{(0)} &= \begin{pmatrix} 0 & 0 & 0 & 0 & 0 & 0 & 0 & 0 & 0 \\ 0 & 0 & 0 & 0 & 0 & 0 & 0 & 0 & 0 \\ 0 & 0 & 1 & 0 & -1 & 0 & 1 & 0 & 0 \\ 0 & 0 & 0 & 0 & 0 & 0 & 0 & 0 & 0 \\ 0 & 0 & -1 & 0 & 1 & 0 & -1 & 0 & 0 \\ 0 & 0 & 0 & 0 & 0 & 0 & 0 & 0 & 0 \\ 0 & 0 & 1 & 0 & -1 & 0 & 1 & 0 & 0 \\ 0 & 0 & 0 & 0 & 0 & 0 & 0 & 0 & 0 \\ 0 & 0 & 0 & 0 & 0 & 0 & 0 & 0 & 0 \end{pmatrix} \\ &= \frac{1}{2} \sum_{i=1}^8 \lambda^i \otimes \tilde{\lambda}^i + \frac{1}{3}. \end{aligned} \quad (39)$$

It follows that $\vec{\lambda}_x \cdot \vec{\lambda}_y$ is left invariant by U_Λ whenever $x \in \Lambda_A, y \in \Lambda_B$. From Eq. (18), $\vec{\lambda}_x \cdot \vec{\lambda}_y$ is also left invariant whenever x, y belong to the same sublattice. The loop representation differs from the one for $J_1 = J_2$ but the joint distribution of macroscopic loops is the same PD(3).

E. Antiferromagnetic phase

The extremal states are indexed by unit vectors \vec{a} in \mathbb{R}^3 . If the lattice is bipartite they can be defined using the usual staggered fields, namely

$$\langle \cdot \rangle_{\vec{a}}^{\text{AF}} = \lim_{h \rightarrow 0^+} \lim_{\Lambda \rightarrow \mathbb{Z}^d} \langle \cdot \rangle_{H_\Lambda - h \sum_{x \in \Lambda} (-1)^x \vec{a} \cdot \vec{S}_x}. \quad (40)$$

The decomposition reads

$$\langle \cdot \rangle = \int_{\mathbb{S}^2} \langle \cdot \rangle_{\vec{a}}^{\text{AF}} d\nu(\vec{a}). \quad (41)$$

The justification for this formula is quite identical to that of (15) in the ferromagnetic regime. Loops are different but the joint distribution of macroscopic loops is the same PD(2).

Notice that, for $J_1 < 0$, the random loop representation is only valid when the lattice is bipartite. There are problematic signs otherwise. The study of frustrated systems is notoriously difficult.

F. Staggered nematic phase

We conclude this section with a conjecture about the likely extremal states in the region $J_2 < J_1 < 0$. The study of product states in Sec. II suggests that each edge consists of a nematic state, and of a state that is perpendicular with respect to the scalar product in \mathbb{C}^3 . On a bipartite lattice one gains entropy by choosing a given nematic state on all sites of a sublattice; this allows one to choose independent perpendicular states on the sites of the other sublattice. We saw in Sec. III C that $|0\rangle$ seems better. This suggests the following extremal states: if $\vec{a} \in \mathbb{S}_+^2$,

$$\langle \cdot \rangle_{\vec{a}}^{\text{st nematic}} = \lim_{h \rightarrow 0^+} \lim_{\Lambda \rightarrow \mathbb{Z}^d} \langle \cdot \rangle_{H_\Lambda + h \sum_x (-1)^x (\vec{a} \cdot \vec{S})^2}. \quad (42)$$

And if $\vec{a} \in \mathbb{S}_-^2$, $\langle \cdot \rangle_{\vec{a}}^{\text{st nematic}}$ is as above but with $h \rightarrow 0^-$. In the first case, nematic order occurs on the sublattice that contains the origin; in the second case, order occurs on the other sublattice.

There exist random loop representations for these parameters, but they carry signs and therefore do not offer evidence for the conjecture (42).

IV. RANDOM LOOP REPRESENTATION FOR THE NEMATIC AND SU(3) REGIONS

The partition function of quantum lattice models can be expanded using the Trotter product formula, or the Duhamel formula, yielding a sort of classical model in one more dimension. For some models the expansion takes the form of random loops. This turns out to be important for our purpose.

Random loop models were used in studies of the spin- $\frac{1}{2}$ Heisenberg ferromagnet [17,18] and of the antiferromagnet [19]. An extension was proposed recently [11] that applies to the spin- $\frac{1}{2}$ XY model, and to the spin-1 model in the nematic and SU(3) regions $0 \leq J_1 \leq J_2$. We describe it in detail in this

section. A more complicated class of loop models that applies to the half-plane $J_2 \geq 0$ will be introduced in the next section.

Recall the transposition operator T_{xy} in Eq. (3), the projector onto the spin singlet $P_{xy}^{(0)}$ in (4), and their relations with spin operators in (5). We consider convex combinations of these operators. Namely, we consider the family of Hamiltonians

$$\begin{aligned} H_\Lambda &= - \sum_{\langle x,y \rangle} (u T_{xy} + (1-u) P_{xy}^{(0)} - 1) \\ &= - \sum_{\langle x,y \rangle} (u \vec{S}_x \cdot \vec{S}_y + (\vec{S}_x \cdot \vec{S}_y)^2 - 2). \end{aligned} \quad (43)$$

Next, recall that a Poisson point process on the interval $[0, 1]$ describes the occurrence of independent events at random times. Let $u \geq 0$ be the intensity of the process. The probability that an event occurs in the infinitesimal interval $[t, t + dt]$ is $u dt$; disjoint intervals are independent. Poisson point processes are relevant to us because of the following expansion of the exponential of matrices:

$$\exp \left\{ u \sum_{i=1}^k (M_i - 1) \right\} = \int \rho(d\omega) \prod_{(i,t) \in \omega} M_i, \quad (44)$$

where ρ is a Poisson point process on $\{1, \dots, k\} \times [0, 1]$ with intensity u , and the product is over the events of the realization ω in increasing times. We actually consider an extension where the time intervals are labeled by the edges of the lattice, and where two kinds of events occur with respective intensities u and $1 - u$. Then

$$\begin{aligned} \exp \left\{ - \sum_{\langle x,y \rangle} (u M_{xy}^{(1)} + (1-u) M_{xy}^{(2)} - 1) \right\} \\ = \int \rho(d\omega) \prod_{(x,y,i,t) \in \omega} M_{xy}^{(i)}. \end{aligned} \quad (45)$$

The product is over the events of ω in increasing times; the label i is equal to 1 if the event is of the first kind, and 2 if the event is of the second kind.

Let $|\sigma\rangle = \otimes_{x \in \Lambda} |\sigma_x\rangle$, $\sigma_x \in \{-1, 0, 1\}$, denote the elements of the basis of \mathcal{H}_Λ where S_x^3 are diagonal. Applying the Poisson expansion (45), we get

$$\begin{aligned} \text{Tr} e^{- \sum_{\langle x,y \rangle} [u T_{xy} + (1-u) P_{xy}^{(0)} - 1]} \\ = \int \rho(d\omega) \sum_{|\sigma_1\rangle, \dots, |\sigma_k\rangle} \langle \sigma_1 | M_{x_k y_k}^{(i_k)} | \sigma_k \rangle \langle \sigma_k | M_{x_{k-1} y_{k-1}}^{(i_{k-1})} | \sigma_{k-1} \rangle \\ \dots, \langle \sigma_2 | M_{x_1 y_1}^{(i_1)} | \sigma_1 \rangle. \end{aligned} \quad (46)$$

Here, $(x_1, y_1, i_1), \dots, (x_k, y_k, i_k)$ are the events of the realization ω in increasing times. Their number k is random.

This expansion has a convenient graphical description. Namely, let $d\rho$ denote the measure for a Poisson point process for each edge of Λ , where ‘‘crosses’’ occur with intensity u and ‘‘double bars’’ occur with intensity $1 - u$. In order to find the loop that contains a given point $(x, t) \in \Lambda \times [0, \beta]$, one can start by moving upwards, say, until one meets a cross or a double bar. Then one jumps onto the corresponding neighbor; if the transition is a cross, one continues in the same vertical direction; if it is a double bar, one continues

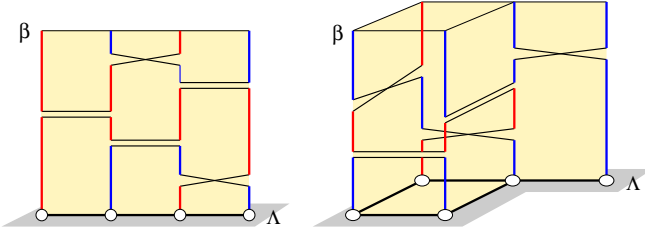


FIG. 2. (Color online) Random loop model for parameters $0 \leq J_1 \leq J_2$. In both figures, the realization has $|\mathcal{L}(\omega)| = 2$ loops.

in the opposite direction. The vertical direction has periodic boundary conditions. See Fig. 2 for illustrations.

The sum over $|\sigma_i\rangle$ is then equivalent to assigning independent labels along each loop. The labels take values in $\{-1, 0, 1\}$ and they are constant along vertical legs. When meeting a cross and jumping onto a neighbor, they stay constant. When meeting a double bar and jumping onto a neighbor, they change sign. In (46) the matrix elements of T_{xy} are equal to 1 if the labels are compatible with the loop and zero otherwise. The matrix elements of $P_{xy}^{(0)}$ are ± 1 if the labels are compatible with the loop and zero otherwise. The number of factors -1 along a given loop is always even, because it is related to the number of changes of vertical directions. Thus the overall factor is 1 and the signs disappear.

Since each loop can have exactly three labels, the partition function is

$$Z_\Lambda = \text{Tr}_{\mathcal{H}_\Lambda} e^{-\beta H_\Lambda} = \int 3^{|\mathcal{L}(\omega)|} \rho(d\omega). \quad (47)$$

Let \mathbb{P} denote the probability with respect to the measure $\frac{1}{Z_\Lambda} 3^{|\mathcal{L}(\omega)|} \rho(d\omega)$. The spin-spin correlation function can be calculated using the same expansion as for the partition function. We get

$$\text{Tr} S_x^3 S_y^3 e^{-\beta H_\Lambda} = \int \rho(d\omega) \sum_{\sigma:\omega} \sigma_x \sigma_y. \quad (48)$$

The sum is over all possible labels for the loops, and σ_x denotes the label at site x and time zero. The sum is zero unless x and y belong to the same loop (at time zero), in which case it gives $\pm \frac{2}{3} 3^{|\mathcal{L}(\omega)|}$. The sign depends on whether the loop reaches y from below or from above. We find therefore

$$\langle S_x^i S_y^i \rangle_{H_\Lambda} = \frac{2}{3} \left[\mathbb{P} \left(x \begin{array}{c} \diagup \diagdown \\ \diagdown \diagup \end{array} y \right) - \mathbb{P} \left(x \begin{array}{c} \text{---} \\ \text{---} \end{array} y \right) \right]. \quad (49)$$

The first event refers to loops that connect the top of x to the bottom of y ; the second event refers to loops that connect the top of x with the top of y . This expression is actually very interesting and suggests that the spin-spin correlation function has exponential decay in the nematic phase, for all temperatures. The quadrupolar correlation function can also be calculated [11] and it is proportional to the probability that both sites (at time zero) belong to the same loop:

$$\langle A_x A_y \rangle_{H_\Lambda} = \frac{2}{9} \mathbb{P}(x \leftrightarrow y). \quad (50)$$

V. RANDOM LOOP REPRESENTATIONS FOR $J_2 \geq 0$

We now describe a more general class of loop models that apply to the upper half of the phase diagram, $J_2 \geq 0$. These

loop models were proposed by Nachtergaele [20,21] and independently by Harada and Kawashima [22]. In the region $J_1 < 0$, the lattice must be bipartite in order for the signs to be positive.

A. Transition operators

Consider a system where each site $x \in \Lambda$ hosts two spins $\frac{1}{2}$. The Hilbert space is $\mathcal{H}'_\Lambda = \otimes_{x \in \Lambda} (\mathbb{C}^2 \otimes \mathbb{C}^2)$. Let \mathcal{S} be the projector onto the triplet subspace in $\mathbb{C}^2 \otimes \mathbb{C}^2$,

$$\mathcal{S}|a, b\rangle = \frac{1}{2}|a, b\rangle + \frac{1}{2}|b, a\rangle, \quad (51)$$

and let

$$\mathcal{S}_x = \mathcal{S} \otimes \mathbb{1}_{\Lambda \setminus \{x\}}, \quad \mathcal{S}_\Lambda = \otimes_{x \in \Lambda} \mathcal{S}. \quad (52)$$

Let $V : \mathbb{C}^3 \rightarrow \mathbb{C}^2 \otimes \mathbb{C}^2$ be the operator such that

$$\begin{aligned} V^* V &= \mathbb{1}_{\mathbb{C}^3}, \\ V V^* &= \mathcal{S}. \end{aligned} \quad (53)$$

Define the operators on $\mathbb{C}^2 \otimes \mathbb{C}^2$ by

$$T^i = V S^i V^*, \quad i = 1, 2, 3, \quad (54)$$

where the S^i 's are the spin operators in \mathbb{C}^3 . One can check that the T^i 's satisfy the following relations:

$$\begin{aligned} [T^1, T^2] &= iT^3 \quad (\text{and cyclic relations}), \\ (T^1)^2 + (T^2)^2 + (T^3)^2 &= 2\mathcal{S}. \end{aligned} \quad (55)$$

These operators can be written with the help of Pauli matrices. Namely,

$$\begin{aligned} T^i &= (\sigma^i \otimes \mathbb{1} + \mathbb{1} \otimes \sigma^i) \mathcal{S} \\ &= 2\mathcal{S}(\sigma^i \otimes \mathbb{1}) \mathcal{S}. \end{aligned} \quad (56)$$

Notice that $\sigma^i \otimes \mathbb{1} + \mathbb{1} \otimes \sigma^i$ commutes with \mathcal{S} .

Using the operators above, we define the following Hamiltonian on \mathcal{H}'_Λ :

$$H'_\Lambda = - \sum_{(x,y)} (J_1 \vec{T}_x \cdot \vec{T}_y + J_2 (\vec{T}_x \cdot \vec{T}_y)^2). \quad (57)$$

The partition function and the Gibbs states are defined by

$$\begin{aligned} Z'_\Lambda &= \text{Tr}_{\mathcal{H}'_\Lambda} \mathcal{S}_\Lambda e^{-\beta H'_\Lambda}, \\ \langle A' \rangle_{H'_\Lambda} &= \frac{1}{Z'_\Lambda} \text{Tr} A' \mathcal{S}_\Lambda e^{-\beta H'_\Lambda}. \end{aligned} \quad (58)$$

The correspondence between the spin-1 model H_Λ and the new model H'_Λ is then

$$\langle A \rangle_{H_\Lambda} = \langle V_\Lambda A V_\Lambda^* \rangle_{H'_\Lambda}. \quad (59)$$

We need to rewrite the Hamiltonian H'_Λ using suitable operators in order to get the loop representations. We use symbols that are suggestive of the two sites of two spins each, and of the links due to transitions. We also use the notation $|a, b\rangle$ for an element in the one-site Hilbert space $\mathbb{C}^2 \otimes \mathbb{C}^2$, and $|a, b\rangle \otimes |c, d\rangle$ for an element in the two-site Hilbert space.

With these conventions in mind, let

$$\begin{aligned} \mathcal{H}' |a, b\rangle \otimes |c, d\rangle &= |c, b\rangle \otimes |a, d\rangle, \\ \mathcal{X}' |a, b\rangle \otimes |c, d\rangle &= |c, d\rangle \otimes |a, b\rangle. \end{aligned} \quad (60)$$

These are transposition operators for one or two spins. We actually need the symmetrized operators

$$\mathcal{H} = \mathcal{S}_{x,y} \mathcal{H}' \mathcal{S}_{x,y}, \quad \mathcal{X} = \mathcal{S}_{x,y} \mathcal{X}' \mathcal{S}_{x,y}. \quad (61)$$

They can be written in terms of spin operators as follows:

$$\begin{aligned} \mathcal{H} &= \frac{1}{2} \vec{T}_x \cdot \vec{T}_y + \frac{1}{2} \mathcal{S}_{x,y}, \\ \mathcal{X} &= \vec{T}_x \cdot \vec{T}_y + (\vec{T}_x \cdot \vec{T}_y)^2 - \mathcal{S}_{x,y}. \end{aligned} \quad (62)$$

Next, let us consider the operators that are related to spin singlets at distinct sites:

$$\begin{aligned} \langle a', b' | \otimes \langle c', d' | \mathcal{H}' |a, b\rangle \otimes |c, d\rangle \\ = (-1)^{a-a'} (-1)^{b-b'} \delta_{a,-d} \delta_{b,-c} \delta_{a',-d'} \delta_{b',-c'}, \\ \langle a', b' | \otimes \langle c', d' | \mathcal{X}' |a, b\rangle \otimes |c, d\rangle \\ = (-1)^{b-b'} \delta_{a,a'} \delta_{d,d'} \delta_{b,-c} \delta_{b',-c'}. \end{aligned} \quad (63)$$

We again need the symmetrized operators

$$\mathcal{H} = \mathcal{S}_{x,y} \mathcal{H}' \mathcal{S}_{x,y}, \quad \mathcal{X} = \mathcal{S}_{x,y} \mathcal{X}' \mathcal{S}_{x,y}. \quad (64)$$

In terms of spin operators, they are given by

$$\begin{aligned} \mathcal{X} &= (\vec{T}_x \cdot \vec{T}_y)^2 - \mathcal{S}_{x,y}, \\ \mathcal{H} &= -\frac{1}{2} \vec{T}_x \cdot \vec{T}_y + \frac{1}{2} \mathcal{S}_{x,y}. \end{aligned} \quad (65)$$

We can also consider the operator

$$\begin{aligned} \langle a', b' | \otimes \langle c', d' | \mathcal{X}' |a, b\rangle \otimes |c, d\rangle \\ = (-1)^{b-b'} \delta_{a,d'} \delta_{a',d} \delta_{b,-c} \delta_{b',-c'}. \end{aligned} \quad (66)$$

Its symmetrized version satisfies

$$\mathcal{X} = -\frac{1}{2} \vec{T}_x \cdot \vec{T}_y - (\vec{T}_x \cdot \vec{T}_y)^2 + \frac{3}{2} \mathcal{S}_{x,y}. \quad (67)$$

The correspondence between the transition operators and the parameters J_1, J_2 is illustrated in Fig. 3. The Hamiltonian H'_Λ can be written as linear combinations of the transition operators. In order to avoid future sign problems, we choose the following linear combinations. For $0 \leq J_2 \leq J_1$,

$$H'_\Lambda = - \sum_{\langle x,y \rangle} \left(2(J_1 - J_2) \mathcal{H}' + J_2 \mathcal{X}' + (-J_1 + 2J_2) \mathcal{S}_{x,y} \right); \quad (68)$$

for $0 \leq J_1 \leq J_2$,

$$H'_\Lambda = - \sum_{\langle x,y \rangle} \left((J_2 - J_1) \mathcal{H}' + J_1 \mathcal{X}' + J_2 \mathcal{S}_{x,y} \right); \quad (69)$$

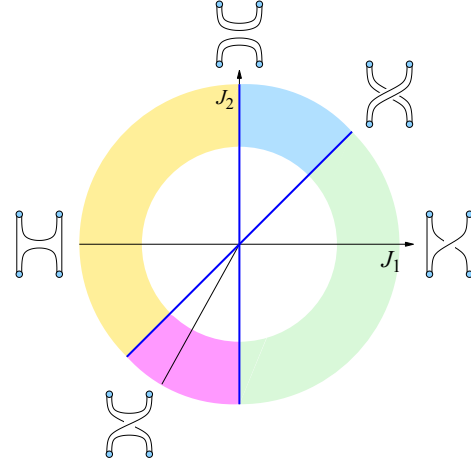


FIG. 3. (Color online) Random loop representations for the different interactions. Convex combinations are possible. The loop representation in the direction $(J_1 = -\frac{1}{2}, J_2 = -1)$, with transition operator (67), carries signs.

and for $J_1 < 0, J_2 \geq 0$,

$$H'_\Lambda = - \sum_{\langle x,y \rangle} \left(-2J_1 \mathcal{H}' + J_2 \mathcal{X}' + (J_1 + J_2) \mathcal{S}_{x,y} \right). \quad (70)$$

B. Nachtergaele's loop representations

Let $|\sigma\rangle = \otimes_{x \in \Lambda} |\sigma_x^{(1)}, \sigma_x^{(2)}\rangle$, $\sigma_x^{(i)} = \pm \frac{1}{2}$, denote the elements of the basis of \mathcal{H}'_Λ where all $(\sigma^3 \otimes \mathbb{1})_x$ and $(\mathbb{1} \otimes \sigma^3)_x$ are diagonal. We can again use (45) and we obtain an expansion that is similar to (46). Because of the properties of the transition operators, the expansion has graphical interpretation.

Let us examine the case of the Hamiltonian H'_Λ for $0 \leq J_2 \leq J_1$, given in Eq. (68). We can neglect the term $(-J_1 + 2J_2) \mathcal{S}_{x,y}$ and add $2J_1 + J_2$ times the identity so that we can use the Poisson expansion formula (45). Indeed, this may change the partition function, but it does not change the Gibbs states. A realization can then be represented as in Fig. 4. There are two vertical lines on top of each site and neighboring lines are sometimes connected by the transitions. The little boxes represent the action of the symmetrization operator \mathcal{S}_x in Eq. (51), namely to average over an identity

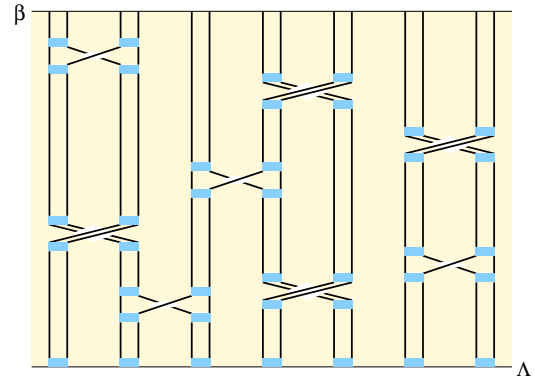


FIG. 4. (Color online) Realization of the Poisson point process. The lattice is one-dimensional here but the representation applies to arbitrary dimensions.

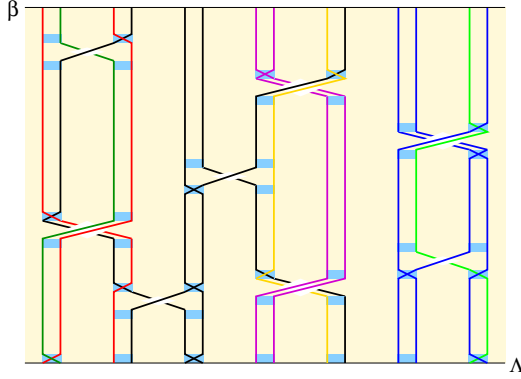


FIG. 5. (Color online) Realization $\bar{\omega}$ and its loop configuration. Here, $|\mathcal{L}(\bar{\omega})| = 7$.

and a transposition. Graphically,

$$\blacksquare = 1/2 \mid \blacksquare + 1/2 \bowtie$$

Let $\bar{\omega}$ denote the realization ω together with a choice of the status of all symmetrization boxes. We keep the notation ρ for the corresponding measure. Loop configurations are obtained by connecting the vertical lines according to the transition symbols. See Fig. 5. The sum over configurations $|\sigma_1\rangle, \dots, |\sigma_k\rangle$ amounts to a choice over assignments of a spin value $\pm \frac{1}{2}$ to each loop. The partition function is then given by

$$Z'_\Lambda = \int \rho(d\bar{\omega}) 2^{|\mathcal{L}(\bar{\omega})|}, \quad (71)$$

where $|\mathcal{L}(\bar{\omega})|$ is the number of loops in the realization $\bar{\omega}$. A similar expansion can be performed for the correlation functions. We find

$$\text{Tr}(\sigma^3 \otimes \mathbb{1})_x (\sigma^3 \otimes \mathbb{1})_y e^{-\beta H'_\Lambda} = \int \rho(d\bar{\omega}) \sum_{\sigma: \bar{\omega}} \sigma_x^{(1)} \sigma_y^{(1)}. \quad (72)$$

If the realization $\bar{\omega}$ does not connect the first lines of the sites x and y , the sum gives zero. If the first lines of x, y belong to the same loop, the sum gives $\frac{1}{4} 2^{|\mathcal{L}(\bar{\omega})|}$. Recalling Eqs. (56) and (59), we get for $0 \leq J_2 \leq J_1$

$$\langle S_x^3 S_y^3 \rangle_{H'_\Lambda} = \langle T_x^3 T_y^3 \rangle_{H'_\Lambda} = \mathbb{P}((x, 1) \leftrightarrow (y, 1)), \quad (73)$$

where the right side is the probability, with measure $\frac{1}{Z'_\Lambda} d\rho$, that the first lines of x and y belong to the same loop.

The situation with transition operators \mathbb{H} and \mathbb{K} is similar but there are two important differences. Indeed, because of the matrix elements of Eqs. (63), we have that the spin value in the loop changes sign at those transitions where the vertical direction changes and there are extra factors, namely $e^{i\pi a}$ for transitions of the form \square and $e^{-i\pi a}$ for transitions of the form \sqcup , where $a = \pm \frac{1}{2}$ is the value of the spin at sublattice A .

The factors give 1 when the lattice is bipartite and (i) the transitions \mathbb{H} and \mathbb{K} are between distinct sublattices only; (ii) the transpositions are between sites in the same sublattices. Thus \mathbb{H} and \mathbb{K} can be combined with one another, but they cannot be combined with \mathbb{H} and \mathbb{K} . Actually, it is possible to combine \mathbb{K} and \mathbb{K} for the nematic phase. But in this case we

can also use the simpler loop representation of Sec. IV where each site has a single line.

The partition function for the Hamiltonian H'_Λ in (70) is again $Z'_\Lambda = \int \rho(d\bar{\omega}) 2^{|\mathcal{L}(\bar{\omega})|}$. As for correlation functions, Eq. (72) holds with the new notion of loops. The sum over $\sigma: \bar{\omega}$ gives (i) zero if the first lines of x, y do not belong to the same loop; (ii) $\frac{1}{4} 2^{|\mathcal{L}(\bar{\omega})|}$ if they belong to the same loop and x, y belong to the same sublattice; (iii) $-\frac{1}{4} 2^{|\mathcal{L}(\bar{\omega})|}$ if they belong to the same loop and x, y belong to different sublattices. Then we find for $J_1 \leq 0, J_2 \geq 0$:

$$\langle S_x^3 S_y^3 \rangle_{H'_\Lambda} = \langle T_x^3 T_y^3 \rangle_{H'_\Lambda} = (-1)^{x-y} \mathbb{P}((x, 1) \leftrightarrow (y, 1)). \quad (74)$$

Let us conclude this subsection by giving two identities. A similar calculation as above gives $\langle (T_x^3)^2 \rangle_{H'_\Lambda} = \frac{1}{2} + \frac{1}{2} \mathbb{P}((x, 1) \leftrightarrow (x, 2))$. Since the first term is equal to $\frac{2}{3}$, we find that

$$\mathbb{P}((x, 1) \leftrightarrow (x, 2)) = \frac{1}{3} \quad (75)$$

for all values of β and of interaction parameters. This should be understood as an effect of the symmetrization operators, which connect the two points with probability $1/3$ (if initially disconnected), or disconnect them with probability $2/3$ (if initially connected). The factor $2^{|\mathcal{L}(\bar{\omega})|}$ is important. Next, we compute the expression for the quadrupolar correlation function. Recall the operator $A_x = (S_x^3)^2 - \frac{2}{3}$. We find

$$\begin{aligned} \langle A_x A_y \rangle_{H'_\Lambda} &= -\frac{1}{36} + \frac{1}{4} \mathbb{P} \left(\begin{array}{cc} (x, 1) & (y, 1) \\ \uparrow & \uparrow \\ (x, 2) & (y, 2) \end{array} \right) \\ &+ \frac{1}{2} \mathbb{P} \left(\begin{array}{cc} (x, 1) & (y, 1) \\ \leftarrow & \leftarrow \\ (x, 2) & (y, 2) \end{array} \right) \\ &+ \frac{1}{4} \mathbb{P} \left((x, 1), (x, 2), (y, 1), (y, 2) \text{ in same loop} \right). \end{aligned} \quad (76)$$

It seems quite equivalent to the spin-spin correlation function (73), and it would be interesting to work out precise comparison. Notice that Eqs. (75) and (76) are valid in the whole region $J_2 \geq 0$.

VI. JOINT DISTRIBUTION OF THE LENGTHS OF LONG LOOPS

A. Macroscopic loops and random partitions

Let $L^{(1)}, L^{(2)}, \dots$ denote the lengths of the loops in decreasing order. Here, the “length” of the loop is by definition the sum of lengths of its vertical components; thus $0 \leq L^{(i)} \leq \beta |\Lambda|$ and $\sum_i L^{(i)} = \beta |\Lambda|$. We expect the largest ones to be of order of the volume, and the smaller ones to be of the order of unity. We actually expect that the following limit exists for almost all realizations of loop configurations:

$$\lim_{k \rightarrow \infty} \lim_{\Lambda \rightarrow \mathbb{Z}^d} \sum_{i=1}^k \frac{L^{(i)}}{\beta |\Lambda|} = m(\beta). \quad (77)$$

Further, we expect that the limit $m = m(\beta)$ takes a fixed value. The order of limits is of course important, the result is trivially 1 if the order is reversed. Next, in the limits $\Lambda \rightarrow \mathbb{Z}^d$ then $k \rightarrow \infty$, the sequence $(\frac{L^{(1)}}{\beta |\Lambda|}, \frac{L^{(2)}}{\beta |\Lambda|}, \dots)$ is a random partition of $[0, 1]$. It turns out that its probability measure can be

described explicitly; it is a Poisson-Dirichlet distribution $\text{PD}(\theta)$ for a suitable parameter $\theta > 0$.

Aldous conjectured that $\text{PD}(1)$ occurs in the random interchange model on the complete graph; this was proved by Schramm [23], who showed that the time evolution of the loop lengths is described by an effective split-merge process (or ‘‘coagulation fragmentation’’). The random interchange model is equivalent to the random loop model of Sec. IV without the factor $3^{|\mathcal{L}(\omega)|}$. It was later understood that the Poisson-Dirichlet distribution is also present in three-dimensional systems [13]. This behavior is actually fairly general and concerns many systems where one-dimensional objects have macroscopic size. The distribution $\text{PD}(1)$ has been confirmed numerically in a model of lattice permutations [24] and analytically in the related annealed model [25]. More general $\text{PD}(\theta)$ have been confirmed numerically in $O(n)$ loop models [14].

There are several definitions of Poisson-Dirichlet distributions. The simplest one is through the Griffiths-Engen-McCloskey (GEM) distribution. Let X_1, X_2, \dots be independent identically distributed Beta(θ) random variables. That is, each X_i takes value in $[0, 1]$ and $\mathbb{P}(X > s) = (1 - s)^\theta$ for $0 \leq s \leq 1$. The following is a random partition of $[0, 1]$:

$$(X_1, (1 - X_1)X_2, (1 - X_1)(1 - X_2)X_3, \dots).$$

The corresponding distribution is called $\text{GEM}(\theta)$. After reordering the numbers in decreasing order, the resulting random partition has $\text{PD}(\theta)$ distribution.

The probability that two random numbers, chosen uniformly in $[0, 1]$, belong to the same element in $\text{PD}(\theta)$, can be calculated with $\text{GEM}(\theta)$. They both belong to the k th element with probability

$$\mathbb{E}((1 - X_1)^2 \dots (1 - X_{k-1})^2 X_k^2) = \mathbb{E}((1 - X_1)^2)^{k-1} \mathbb{E}(X_1^2). \quad (78)$$

We have $\mathbb{E}((1 - X_1)^2) = \theta/(\theta + 2)$ and $\mathbb{E}(X_1^2) = 2/(\theta + 1)$ ($\theta + 2$). Summing over k , we find that the probability that two random numbers belong to the same element is equal to $1/(\theta + 1)$.

B. Effective split-merge process

The strategy is to view the random loop measure as the stationary measure of a suitable stochastic process. The effective process on random partitions is a split-merge process with suitable rates. Then its invariant measure is a $\text{PD}(\theta)$ distribution with θ that depends on the rates.

We consider the simpler loop model of Sec. IV and explain later that modifications are minimal for the other loop models. Let $R(\omega, \omega')$ be the transition matrix of the stochastic process that gives the rate at which ω' occurs when the configuration is ω . With $C(\omega)$ the number of crosses and $B(\omega)$ the number of double bars, the detailed balance property is

$$\begin{aligned} & 3^{|\mathcal{L}(\omega)|} (u dt)^{C(\omega)} ((1 - u) dt)^{B(\omega)} R(\omega, \omega') \\ &= 3^{|\mathcal{L}(\omega')|} (u dt)^{C(\omega')} ((1 - u) dt)^{B(\omega')} R(\omega', \omega). \end{aligned} \quad (79)$$

We have discretized the interval $[0, \beta]$ with mesh dt . The following process satisfies the detailed balance property.

(i) A new cross appears in the interval $[x, y] \times [t, dt]$ at rate $\sqrt{3} u dt$ if its appearance causes a loop to split, at rate

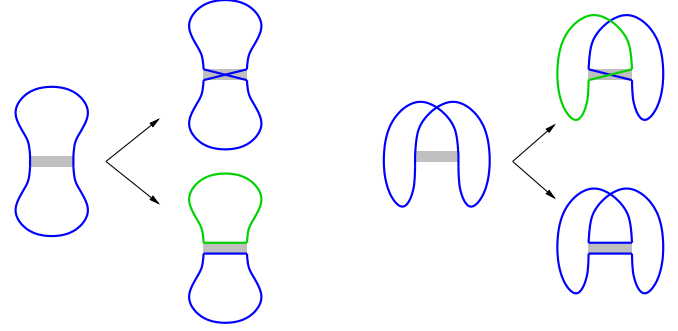


FIG. 6. (Color online) When $u \in (0, 1)$, a local change involving two legs of the same loop may rearrange it rather than split it. This figure shows all cases corresponding to the addition of a transition. The loop necessarily splits when $u = 1$, and also when $u = 0$ on a bipartite graph.

$(u/\sqrt{3})dt$ if its appearance causes two loops to merge, and at rate $u dt$ if its appearance does not modify the number of loops.

(ii) Same with bars, but with rate $1 - u$ instead of u .

(iii) An existing cross and double bar is removed at rate $\sqrt{3}$ if its removal causes a loop to split, at rate $1/\sqrt{3}$ if its removal causes two loops to merge, and at rate 1 if the number of loops remains constant.

Notice that any new cross or double bar between two loops causes them to merge. When $u = 1$, any new cross within a loop causes it to split.

Let γ, γ' be two macroscopic loops of respective lengths L, L' . They are spread all over Λ and they interact between one another, and among themselves, in an essentially mean-field fashion. There exists a constant c_1 such that a new cross or double bar that causes γ to split appears at rate $\frac{1}{2}\sqrt{3}c_1 \frac{L^2}{\beta|\Lambda|}$; a new cross or double bar that causes γ and γ' to merge appears at rate $(c_1/\sqrt{3}) \frac{LL'}{\beta|\Lambda|}$. There exists another constant c_2 such that the rate for an existing cross or double bar to disappear is $\frac{1}{2}\sqrt{3}c_2 \frac{L^2}{\beta|\Lambda|}$ if γ is split, and $(c_2/\sqrt{3}) \frac{LL'}{\beta|\Lambda|}$ if γ and γ' are merged. Consequently, γ splits at rate

$$\frac{1}{2}\sqrt{3}(c_1 + c_2) \frac{L^2}{\beta|\Lambda|} \equiv \frac{1}{2}r_s L^2 \quad (80)$$

and γ, γ' merge at rate

$$\frac{1}{\sqrt{3}}(c_1 + c_2) \frac{LL'}{\beta|\Lambda|} \equiv r_m LL'. \quad (81)$$

Because of effective averaging over the whole domain, the constants c_1 and c_2 are the same for all loops and for both the split and merge events. This key property is certainly not obvious and the interested reader is referred to a detailed discussion for lattice permutations with numerical checks [24]. It follows that the lengths of macroscopic loops satisfy an effective split-merge process, and the invariant distribution is Poisson-Dirichlet with parameter $\theta = r_s/r_m = 3$ [13,26].

The case $u \in (0, 1)$ is different because loops split with only half the rate above. Indeed, the appearance of a new transition within the loop may just rearrange it: topologically, this is like $0 \leftrightarrow 8$; see Fig. 6 for illustration. This yields $\text{PD}(\frac{3}{2})$. Notice

that this cannot happen when $u = 1$, or when $u = 0$ on a bipartite graph.

It follows from these considerations that the macroscopic loops of the model described in Sec. IV have the following Poisson-Dirichlet distributions: PD(3) when $J_1 = J_2 > 0$ and when $J_1 = 0, J_2 > 0$; PD($\frac{3}{2}$) when $0 < J_1 < J_2$.

If the graph is not bipartite, it is still PD(3) when $J_1 = J_2 > 0$, but it is PD($\frac{3}{2}$) otherwise, including when $J_1 = 0, J_2 > 0$.

The heuristics for the more complicated loop models of Sec. VB is similar. It helps to reformulate the setting, by considering transitions that connect any vertical lines; this allows one to neglect the symmetrization boxes (except at time zero). The discussion for transitions \mathbb{M} or \mathbb{H} is then as before and the distribution is PD(2).

The transitions \mathbb{X} and \mathbb{Y} have multiple connections and the argument is a bit more difficult. But it is possible to obtain an effective split-merge process where two changes occur in succession, with the appropriate rates. Hence PD(2) again. It is essential for the heuristics that, if two vertical lines at the same site belong to macroscopic loops, they are uncorrelated. This seems to fail because of (75). But this holds since symmetrization boxes are discarded.

This heuristics *does not* apply if the model has only transitions \mathbb{X} (or \mathbb{Y}). Indeed, there are nontrivial correlations between lines at the same site. It should be possible to modify the argument so as to identify the correct Poisson-Dirichlet. But this is not necessary since we can use the simpler loop model of Sec. IV.

C. Long-range correlation in models of random loops

At low temperatures, our large system contains many loops, that are either macroscopic or microscopic. (Mesoscopic loops have vanishing density.) While the lengths of macroscopic loops varies, their total density is essentially fixed and is denoted $m(\beta)$. The probability that two distant points belong to the same loop is then equal to the probability that they both belong to macroscopic loops $m(\beta)^2$, times the probability that they belong to the same partition element. If the random partition has Poisson-Dirichlet distribution with parameter θ , this probability is $1/(\theta + 1)$ and we find therefore

$$\mathbb{P}(x \leftrightarrow y) = \frac{m(\beta)^2}{\theta + 1}. \quad (82)$$

Let us insist that this equation is meant as an identity in the limits $\Lambda \rightarrow \mathbb{Z}^d$ and $\|x - y\| \rightarrow \infty$.

The recent article of Völl and Wessel on the ground state of the model in the triangular lattice [27] allows us to confront the above heuristics with numerical results. Namely, the black curve in their Fig. 1 is proportional to the length of the loop that contains a given point. At $J_1 = J_2$ (this corresponds to $\vartheta = -\frac{3}{4}\pi$ in [27]) it is equal to $m(\beta)/(3 + 1)$; for $J_1 \leq J_2$ (larger ϑ in [27]) it is equal to $m(\beta)/(\frac{3}{2} + 1)$. The discontinuity of the black curve at $J_1 = J_2$ is characterized by the ratio of the above values, i.e., $8/5$. The numerical data from the figure gives a ratio that is roughly equal to $2.6/1.6$, which is indeed remarkably close.

We now calculate the long-distance correlations in the various phases. In the ferromagnetic phase, we have $\theta = 2$. Combining Eqs. (73) and (82), we get that the left side of (16)

is equal to

$$\langle S_x^3 S_y^3 \rangle_{H_\Lambda} = \mathbb{P}((x, 1) \leftrightarrow (y, 1)) \xrightarrow[\|x-y\| \rightarrow \infty]{\Lambda \rightarrow \mathbb{Z}^d} \frac{1}{3} m(\beta)^2. \quad (83)$$

We need an expression for the magnetization of extremal states. It is possible to add an external field of the form $\sum_y T_y^3$ to the Hamiltonian H'_Λ and to perform a similar expansion, using Trotter or Duhamel formulæ. With h positive but tiny, we get that small loops can still carry any spin values, but long loops must have spin value $+\frac{1}{2}$. Consequently,

$$\begin{aligned} \langle S_x^3 \rangle_{\vec{e}_3}^{\text{ferro}} &= \lim_{h \rightarrow 0^+} \lim_{\Lambda \rightarrow \mathbb{Z}^d} \langle T_x^3 \rangle_{H'_\Lambda - h \sum_y T_y^3} \\ &= \lim_{h \rightarrow 0^+} \lim_{\Lambda \rightarrow \mathbb{Z}^d} \langle (2\sigma^3 \otimes \mathbb{1})_x \rangle_{H'_\Lambda - h \sum_y T_y^3} \\ &= m(\beta). \end{aligned} \quad (84)$$

The last line in Eq. (16) is then also equal to $\frac{1}{3} m(\beta)^2$. This confirms the decomposition (15).

Next, we verify the SU(3) decomposition (20). For $J_1 = J_2$, we use the simpler loop representation of Sec. IV. Let $m(\beta)$ be the fraction of sites in macroscopic loops. The distribution is PD(3), so the left side of Eq. (21) is

$$\langle S_x^3 S_y^3 \rangle_{H_\Lambda} = \frac{2}{3} \mathbb{P}(x \leftrightarrow y) \xrightarrow[\|x-y\| \rightarrow \infty]{\Lambda \rightarrow \mathbb{Z}^d} \frac{1}{6} m(\beta)^2. \quad (85)$$

Notice that the same calculation gives

$$\langle \lambda_x^3 \lambda_y^3 \rangle_{H_\Lambda} = \langle \lambda_x^8 \lambda_y^8 \rangle_{H_\Lambda} = \frac{2}{3} \mathbb{P}(x \leftrightarrow y), \quad (86)$$

which justifies the first identity in (21). In the extremal state $\langle \cdot \rangle_{\vec{e}_3}$, long loops have spin value 1 and small loops have any value $-1, 0, +1$. It follows that

$$\langle \lambda_x^3 \rangle_{\vec{e}_3} = m(\beta), \quad \langle \lambda_x^8 \rangle_{\vec{e}_3} = \frac{1}{\sqrt{3}} m(\beta). \quad (87)$$

The last line of (21) is equal to $\frac{1}{6} m(\beta)^2$; this confirms the SU(3) decomposition (20).

Next is the spin nematic phase, for $0 \leq J_1 \leq J_2$. We again use the simpler loop representation; the correct distribution is now PD($\frac{3}{2}$). The quadrupolar correlation function in the symmetric Gibbs state gives

$$\langle A_x A_y \rangle_{H_\Lambda} = \frac{2}{9} \mathbb{P}(x \leftrightarrow y) \xrightarrow[\|x-y\| \rightarrow \infty]{\Lambda \rightarrow \mathbb{Z}^d} \frac{4}{45} m(\beta)^2. \quad (88)$$

This the left side of Eq. (30). The spin values of the long loops of extremal Gibbs states is zero. Thus

$$\langle (S_x^i)^2 - \frac{2}{3} \rangle_{\vec{e}_3}^{\text{nem}} = \begin{cases} \frac{1}{3} m(\beta) & \text{if } i = 1, 2, \\ -\frac{2}{3} m(\beta) & \text{if } i = 3. \end{cases} \quad (89)$$

This implies that the right side of (30) is also equal to $\frac{4}{45} m(\beta)^2$. This confirms that the extremal nematic states are given by Eq. (24), and that the symmetric Gibbs state has the decomposition (25).

The justification of the staggered SU(3) decomposition, Eq. (32), is identical to that of the SU(3) decomposition. And the justification for the antiferromagnetic decomposition (41) is also identical to that of the ferromagnetic decomposition.

To summarize, we have given a precise characterization of the symmetry breakings that occur in a spin-1 quantum model at low temperatures and in dimensions three and higher. We have used random loop representations to confirm the decompositions into extremal Gibbs states. While the present discussion is not rigorous, it is expected to be exact. We have only considered the case $J_2 \geq 0$; a difficult challenge is to

clarify the phase diagram for $J_2 < 0$, and in particular the staggered spin nematic phase.

ACKNOWLEDGMENTS

It is a pleasure to thank Jürg Fröhlich and Gian Michele Graf for long discussions and for key suggestions. I am also grateful to Marek Biskup, John Chalker, Sacha Friedli, Roman Kotecký, Benjamin Lees, Nicolas Macris, Charles-Édouard Pfister, Tom Spencer, and Yvan Velenik for discussions and encouragements. The exposition benefited from useful comments of the two referees.

-
- [1] C.-E. Pfister, *Commun. Math. Phys.* **86**, 375 (1982).
 - [2] J. Fröhlich and C.-E. Pfister, *Commun. Math. Phys.* **89**, 303 (1983).
 - [3] C.-E. Pfister, *Ann. N.Y. Acad. Sci.* **491**, 170 (1987).
 - [4] K. Tanaka, A. Tanaka, and T. Idokagi, *J. Phys. A* **34**, 8767 (2001).
 - [5] K. Harada and N. Kawashima, *Phys. Rev. B* **65**, 052403 (2002).
 - [6] C. D. Batista and G. Ortiz, *Adv. Phys.* **53**, 1 (2004).
 - [7] T. A. Tóth, A. M. Läuchli, F. Mila, and K. Penc, *Phys. Rev. B* **85**, 140403 (2012).
 - [8] Yu. A. Fridman, O. A. Kosmachev, and Ph. N. Klevets, *J. Magn. Magn. Mater.* **325**, 125 (2013).
 - [9] F. J. Dyson, E. H. Lieb, and B. Simon, *J. Stat. Phys.* **18**, 335 (1978).
 - [10] J. Fröhlich, B. Simon, and T. Spencer, *Commun. Math. Phys.* **50**, 79 (1976).
 - [11] D. Ueltschi, *J. Math. Phys.* **54**, 083301 (2013).
 - [12] B. Lees, *J. Math. Phys.* **55**, 093303 (2014).
 - [13] C. Goldschmidt, D. Ueltschi, and P. Windridge, *Contemp. Math.* **552**, 177 (2011).
 - [14] A. Nahum, J. T. Chalker, P. Serna, M. Ortuño, and A. M. Somoza, *Phys. Rev. Lett.* **111**, 100601 (2013).
 - [15] N. Angelescu and V. A. Zagrebnov, *J. Phys. A* **15**, L639 (1982).
 - [16] M. Biskup and L. Chayes, *Commun. Math. Phys.* **238**, 53 (2003).
 - [17] R. T. Powers, *Lett. Math. Phys.* **1**, 125 (1976).
 - [18] B. Tóth, *Lett. Math. Phys.* **28**, 75 (1993).
 - [19] M. Aizenman and B. Nachtergaele, *Commun. Math. Phys.* **164**, 17 (1994).
 - [20] B. Nachtergaele, in *Probability Theory and Mathematical Statistics*, edited by B. Grigelionis *et al.* (VSP/TEV, Utrecht-Tokyo-Vilnius, 1994), p. 565.
 - [21] B. Nachtergaele, in *Probability and Phase Transitions*, edited by G. Grimmett, NATO Advanced Studies Institute, Series C: Mathematical and Physical Sciences (Plenum, New York, 1994), Vol. 420, p. 237.
 - [22] K. Harada and N. Kawashima, *J. Phys. Soc. Jpn.* **70**, 13 (2001).
 - [23] O. Schramm, *Israel J. Math.* **147**, 221 (2005).
 - [24] S. Grosskinsky, A. A. Lovisollo, and D. Ueltschi, *J. Stat. Phys.* **146**, 1105 (2012).
 - [25] V. Betz and D. Ueltschi, *Electron. J. Probab.* **16**, 1173 (2011).
 - [26] J. Bertoin, *Random Fragmentation and Coagulation Processes*, Cambridge Studies Adv. Math. 102 (Cambridge University Press, Cambridge, UK, 2006).
 - [27] A. Völl and S. Wessel, *Phys. Rev. B* **91**, 165128 (2015).